ELSEVIER

Polymer 43 (2002) 781–795

polymer

www.elsevier.com/locate/polymer

Polypropylene blends with potential as materials for microporous membranes formed by melt processing

C. Chandavasu[a], M. Xanthos[a,b,*], K.K. Sirkar[a], C.G. Gogos[a,b]

[a]*Department of Chemical Engineering/Center for Membrane Technologies, New Jersey Institute of Technology, Newark, NJ 07102, USA*
[b]*Polymer Processing Institute, GITC Building, Suite 3901, New Jersey Institute of Technology, Newark, NJ 07102, USA*

Received 9 July 2001; received in revised form 21 September 2001; accepted 24 September 2001

Abstract

Novel microporous membranes with pore size ranging from 2 to 25 nm were produced from immiscible polypropylene blends via melt processing and post-extrusion treatments. Systems containing polystyrene and polyethylene terephthalate as the minor phase components were employed as starting membrane materials at concentrations not exceeding 15 wt%. The blends were first compounded in a co-rotating twin-screw extruder and subsequently extruded through a sheet die to obtain the non-porous precursor films. These were uniaxially drawn (100–500%) with respect to the original dimensions at a temperature below the glass transition temperature of the minor phase to induce a microporous structure and then post-treated at elevated temperatures to stabilize the porous structure, which consisted of uniform microcracks in the order of a few nanometers in width. The effects of dispersed phase concentration and component melt rheology on the solid and microporous blend morphologies are presented. Finite element modeling of the stretching operation in the solid state yielded a successful interpretation of the blend response to uniaxial tension that resulted in microcrack formation. The processes developed in this work may be considered as solventless alternatives to phase inversion manufacturing practices for membranes containing mesopores.

Keywords: Polymer blends; Microporous membranes; Melt processing

1. Introduction

In recent years, porous membranes have been extensively used in commercial processes for gas and liquid separations, wastewater treatment, etc. The driving force and the membrane morphology are the main controlling factors for mass transport of a species across the membrane in a given separation process. According to IUPAC (1985), pore sizes can be formally categorized into three classes; macropores (pore size >50 nm), mesopores (2 nm $<$ pore size $<$ 50 nm), micropores (pore size $<$ 2 nm). The term 'microporous' is used in conventional membrane literature and commercial practice to cover mesopores as well as macropores. It will also be used as a general adjective in this article, which describes a novel and generally applicable technique for the formation of membranes containing mesopores from immiscible polymer blends.

Porous/microporous polymeric membranes are conventionally produced by phase inversion processes that use solvents to dissolve, usually, amorphous polymers. These membranes are not always able to withstand severe chemical environments and high temperatures due to the very nature of the process employed in their preparation. The relatively large pore size of some of these membranes (0.02–0.40 μm) does not allow their use in separations of low molecular weight compounds such as biomolecules, where much smaller pore size (~2–30 nm) is required. Thus, they are primarily used for aqueous solutions with limited applications in the chemical, petrochemical and pharmaceutical industries.

Semicrystalline homopolymers having much higher solvent resistance, e.g. polyolefins, have been employed to produce porous/microporous membranes by a process called thermal-induced phase separation (TIPS) involving the base polymer and a high boiling point diluent. Following phase separation, the diluent is extracted with another miscible solvent. The relationships between morphology and system parameters have been systematically studied in a series of articles published in 1991–1993 beginning with a publication by Lloyd et al. [1]. Membranes from semicrystaline polymers have also been produced via methods

* Corresponding author. Address: Polymer Processing Institute, GITC Building, Suite 3901, New Jersey Institute of Technology, Newark, NJ 07102, USA. Tel.: +1-973-642-4585; fax: +1-973-642-4594.
E-mail address: xanthos@adm.njit.edu (M. Xanthos).

0032-3861/02/$ - see front matter
PII: S0032-3861(01)00654-1

Nomenclature

Ca	capillary number (dimensionless)
d	characteristic diameter of the droplet (m)
G	shear modulus (Pa)
G'	storage modulus (Pa)
G''	loss modulus (Pa)
N	number of dispersed droplets
PP	polypropylene
PS	polystyrene
PET	polyethylene terephthalate
T_g	glass transition temperature (K)
δ	phase angle
Γ	surface/interfacial tension (N/m)
$\dot{\gamma}$	shear rate (s^{-1})
η^*	complex viscosity (Pa s)
μ	viscosity (Pa s)
ϕ	interaction parameter, dimensionless
x^P	polarity
ω	frequency

involving melt processing and post-extrusion treatments [2–5]. These processes that do not involve solvents may be considered as having lower environmental impact. Pores are introduced by stretching the non-porous semi-crystalline polymer precursor film, in the solid state. Examples include Celgard™ polypropylene and Gore-Tex™ polytetrafluoroethylene. Size of pores and overall porosity are controlled by the microstructure of the polymer. In unfilled polypropylene, the membrane range of pore sizes is limited to the dimensions of the crystalline domains of the polymer since pores are induced by either the spreading of the lamellar structure [2–5] or via the β–α crystalline transformation [6,7]. Fine circular pores (0.05 μm) with narrow size distribution have been produced by biaxial stretching of high β-content PP precursor film [8,9]. Slit-like pores are typically 0.20 μm in length and 0.02 μm in width with total porosity of about 30–40% [10]. In certain mineral filled polyolefins, pore size is larger and determined by the stress concentrating characteristics of the finely dispersed filler, which debonds upon the application of stress [11].

To our knowledge, there are no reports on membranes having pore size ranging from 2 to 50 nm (in the lower size range of the ultrafiltration region) which can be used in harsh chemical environment and high temperatures and which are produced from multicomponent, multiphase polymer systems by melt extrusion followed by post-extrusion treatments. The results reported in this article are part of a larger effort to offer a novel and general strategy to provide solventless alternatives to phase inversion manufacturing practices for membranes containing mesopores. Immiscible polymer blends as the starting membrane materials are expected to offer more latitude over single component polymers in achieving the desired pore size and porosity during stretching, since a variety of blend microstructures could be achieved through processing and control of interfacial chemistry. Preliminary results reported in our earlier short communications [12,13] suggest that it is indeed feasible to develop symmetric porous flat film membranes from non-porous precursors by melt processing and subsequent stretching of polypropylene-based blends. Such membranes may have large potential for a number of applications in areas including ultrafiltration, separators in energy systems, sensor technology and other separation processes.

In the present article, we report results obtained with binary polypropylene blends. Results on ternary systems in the presence of additional compatibilizers are reported in separate publications [14,15]. The adopted approach in this work is as follows:

(a) *Preparation and characterization of precursor films*. Selection of polypropylene-based immiscible blend systems, with different component rheological properties (viscosity ratio, elasticity ratio) and different composition, as starting membrane materials and examination of morphologies after melt mixing under different operating conditions. Polystyrene and polyethylene terephthalate were selected as minor blend components representing materials with different crystallinity and thermal transition temperatures.
(b) *Preparation and characterization of mesoporous membranes by post-extrusion drawing*. Investigation of post processing conditions, examination of membrane morphology and evaluation of select transport characteristics. Fundamental studies on the understanding of the development of the membrane morphology and its relation to the non-porous precursor film microstructure.

2. Experimental

2.1. Materials

The materials used as blend components include two polypropylene (PP) homopolymers (PF-100 and PF-814, Montell), polystyrene (PS) (685D, Dow Chemicals) and polyethylene terephthalate (PET), (Shell 9506). When not available, the melt index of the resins was measured according to ASTM D1238 method using a melt index apparatus model CS-127E (Custom Scientific Instruments, Inc.) under standard conditions of temperature and pressure. Properties of the four resins are given in Table 1. Blend components were mixed at different ratios to produce model systems consisting of polypropylene/polyester combinations based on PF100 and two polypropylene/polystyrene compositions based on PF814 and PF100, respectively.

2.2. Melt processing

2.2.1. Extrusion compounding

Polypropylene/polyester (PP-PF100/PET-9506) and

Table 1
Properties of materials used in the study

Polymer	Grade	Source	Density[a] (g/cm^3)	Melt index (g/10 min)
Polypropylene, PP	PF100	Montell Polyolefins	0.90	2.1[a] (230°C/2.16 kg)
	PF814	Montell Polyolefins	0.91	3.7[b] (230°C/2.16 kg)
Polystyrene, PS	685D	Dow Chemicals	1.04	1.5[a] (200°C/5.00 kg)
Polyethylene terephthalate, PET	9506	Shell Chemicals	1.35	10.4[b] (260°C/2.16 kg)

[a] Obtained from supplier's data.
[b] Measured.

polypropylene/polystyrene (PP-PF100/PS-685D and PP-PF814/PS-685D) blends were melt compounded in a 27 mm diameter intermeshing co-rotating twin-screw extruder with length to diameter ratio of 35:1 (Leistritz LSM-30). PET was dried at 90°C under vacuum overnight prior to compounding. The screw configuration consisting of conveying and several mixing elements including kneading blocks can be found in our earlier publications [12,13]. The barrel and die temperature settings were 270°C for the PP-PF100/PET-9506 blend, 230°C for the PP-PF100/PS-685D blend, and 200°C for the PP-PF814/PS-685D blend. The actual melt temperature at the die was measured using a thermocouple. The difference between the temperature setting and the actual melt temperature was within 3°C. The polymers were dry blended and introduced into the hopper of the extruder via a volumetric feeder. The mass feed rate was ranging from 3 to 6 kg/h. In the twin-screw extruder, the materials are subjected to complex shear and elongational deformations, and complex temperature profiles along the various sections of the extruder barrel. However, an effective shear rate may be determined and used as a crude parameter [16]. The effective shear rate of the present extruder was of the order of 60–80 s^{-1}. The blends were melt extruded, chilled, and then collected for morphology observations or pelletized and subsequently used for film extrusion.

The PP-PF100/PS-685D blends were produced at ratios of 90/10, 95/5 and 99/1 wt% to study the effects of the minor phase concentration on the blend morphology. PP-PF814/PS-685D was prepared at 90/10 wt% compositions to compare with the PP-PF100/PS-685D blend in order to elucidate the effects of viscosity ratio on blend morphology. PP-PF100/PET-9506 blends were prepared at 85/15 wt% compositions.

2.2.2. Film extrusion

Non-porous precursor films from pellets produced by the method described above were formed in the Leistritz LSM-30 co-rotating twin-screw extruder equipped with a 10 cm flat sheet die and an extrusion take-off system (C.W. Brabender Instruments, Inc.). The extrusion take-off system consisting of two nip rolls that have a polished smooth surface to prevent surface variation was connected with an oil bath to control temperature by means of heat transfer fluid circulated through the rolls.

In initial experiments films were prepared in a one step operation using a single screw extruder. Two blend systems, 90/10 PF814/PS-685D and 90/10 PF100/PS-685D, were dry-blended and extruded using a 1.9 mm single screw extruder equipped with a general purpose screw and a sheet die (C.W. Brabender Instruments Inc.).

2.2.3. Post-extrusion processing

The microporous membranes were prepared via a series of post-extrusion stretching treatments of the precursor films. In the immiscible blends, dispersed phase domains of the minor component were expected to act as stress concentrators enhancing the local stress within the blend microstructure for the formation of microcracks upon stretching. Microcrack size/distribution would then depend on the dispersed domain size and degree of adhesion at the interface. The post-extrusion treatments included several interrelated steps:

1. The precursor films were uniaxially drawn at a constant rate up to a stretching of 20–30% with respect to the original dimensions at room temperatures ranging from 20 to 25°C to induce interphase crazing by debonding. This post-extrusion drawing was carried out using a Tinius Olsen universal testing machine in a controlled-temperature chamber. The films were drawn at a constant rate ranging from 2.5 to 125 mm/min.
2. The films were subsequently drawn (from 100 up to 500% depending on composition) at temperatures 25–50°C lower than the glass transition temperature of the minor phase by a series of stretching processes. For example, for the PP/PS blend system the draw temperature was 50–75°C to prevent deformation of the minor phase. Films with minor phase concentration exceeding 15 wt% were fairly brittle and could not be easily drawn to high elongations.
3. The films were then treated under tension for about 10 min. at elevated temperatures, 10–20°C lower than the glass transition temperature of the minor phase, to stabilize the porous structure.

2.3. Characterization

2.3.1. Rheological characterization of blend components

Blend components were characterized using a dynamic

mechanical spectrometer (Rheometrics Scientific RMS-800) for complex viscosity (η^*), storage modulus (G'), loss modulus (G'') and dissipation factor (tan δ). The analyses were performed in dynamic mode in either frequency sweep or temperature sweep. In the frequency sweep mode, the material properties were measured at processing temperature conditions using parallel plate fixtures. Frequency was varied from 0.1 to 100 rad/s. Specimens were disks (2.5 cm diameter and 0.5 cm thickness) prepared by compression molding (2 min melting/holding time, 5 min cooling time). Experiments were carried out under dry nitrogen.

2.3.2. Characterization of blend morphology

Scanning electron microscopy is ideally suited to characterize the blend morphology since the variations in size and distribution of the dispersed phase and degree of adhesion could be easily observed using proper sample preparation techniques. In this study, a low voltage field emission scanning electron microscope (Leo 982 FESEM) with a resolution of 1 nm at 30 kV and 4 nm at 1.0 kV was used to determine the blend morphology. At low accelerating voltage, the FESEM provided high resolution imaging with minimal beam damage to the sample. Fracture surfaces and/or microtomed surfaces were examined. Fracture surfaces were prepared at liquid nitrogen temperature and coating was done with a gold/palladium alloy.

Image analysis was used to quantify the size and the size distribution of the minor phase dispersed in the matrix of the major blend component. The electron micrographs were analyzed by the Image-Pro Plus image analysis software (Media Cybernetics) that provides capability for acquiring, enhancing and analyzing images. The diameter (mean) defined as the average length of the diameters measured at two-degree intervals joining two outline points and passing through the centroid of the object was used throughout the study to determine the size and the size distribution of the dispersed phase. Several scanning electron micrographs at different magnifications for each blend system were analyzed. For the characterization of the dispersed phase size, all domains in each micrograph were counted and classified according to their size and shape. About 100–500 domains were scanned with the image analyzer to obtain the size distribution and average diameters. The data were interpreted using a number average dispersed phase dimension, d_n, defined by

$$d_n = \frac{\sum N_i (d_p)_i}{\sum N_i} \quad (1)$$

where N_i is the number of dispersed phase domains with the size $(d_p)_i$.

2.3.3. Membrane characterization

Information on the membrane morphology is one of the requirements to understand and predict its separation performance. In this work, two characterization methods, microscopy and solvent (methanol) permeation, were developed:

2.3.3.1. Electron microscopy. Surface and cross-sectional features of the porous films were examined using the low voltage Leo 982 FESEM to determine morphology including pore size, shape, distribution, surface porosity and three-dimensional structures. The field emission scanning electron microscopy could achieve very high resolution (up to 0.7 nm) even at low beam energy. Accelerating voltage of 0.75–4 kV was used during the examinations. Bulk analyses required the use of microtoming techniques to obtain smooth surfaces of the film cross-section. The sample was first embedded in an epoxy resin, and then cut by a microtome and fixed perpendicular to the sample holder.

2.3.3.2. Liquid permeation. Transport properties of the porous membranes were characterized by permeability measurements of methanol at different applied pressures ranging from 140 to 550 kPa (20–80 psi). A permeation cell was connected to a pressure vessel containing the methanol. Liquid pressurization was achieved by using a nitrogen gas cylinder equipped with a control valve. All plastic tubing used in the experimental setup was Teflon TFE (McMaster–Carr). The liquid was fed to the feed side of the membrane and the permeate was collected at the downstream side of the cell. A schematic of the experimental setup can be found in our earlier publications [12,13].

3. Results and discussion

3.1. Rheological properties of materials

The rheological properties of the materials (Figs. 1–9), although not the emphasis of this article, are important parameters determining the blend morphology. In turn, blend morphology is a very important parameter in determining the membrane morphology. Figs. 1–3 show a system with mismatched rheology. In Fig. 1 the complex viscosity (η^*) vs. frequency (ω) is plotted for the PP-PF814 and the PS-685D at 200°C. In the whole frequency range investigated (0.1–100 rad/s), the PS-685D is more viscous (about 5 times) than the PP-PF814. The viscosities of the PP-PF814 and the PS-685D gradually decrease as the frequency increases. The storage moduli (G') of the PP-PF814 and PS-685D are compared in Fig. 2. The PS-685D is more elastic than the PP-PF814 for the entire frequency range. The loss modulus (G'') curves for the PP-PF814 and PS-685D are shown in Fig. 3.

Figs. 4–6 show a system with matched rheology. In Fig. 4, the complex viscosity is plotted as a function of frequency at 230°C for a different combination of blend components, namely the PP-PF100 and the PS-685D. The dependencies of the storage and loss moduli on frequency at 230°C are

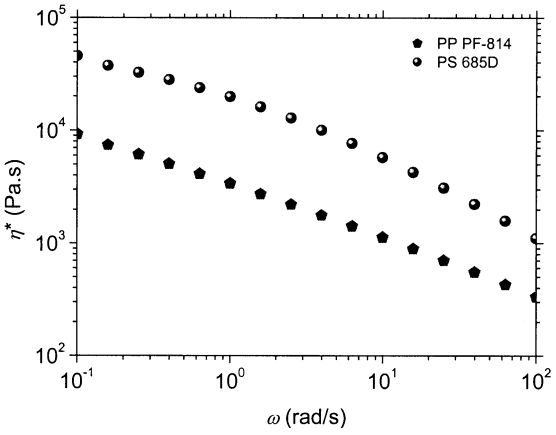

Fig. 1. Plots of complex viscosity (η^*) vs. frequency (ω) of PP-PF814 and PS-685D at 200°C.

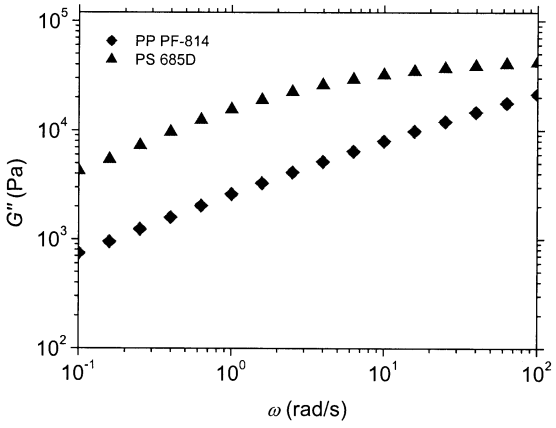

Fig. 3. Plots of loss modulus (G'') vs. frequency (ω) of PP-PF814 and PS-685D at 200°C.

shown in Figs. 5 and 6, respectively. At this temperature, the viscosity and elasticity of PP-PF100 and PS-685D are almost identical for the entire frequency range investigated (0.1–100 rad/s); these are known to be conditions favoring dispersive mixing.

Figs. 7–9 show a system with matched rheology in a narrow shear rate region. The viscosity curves for the PP-PF100 and the PET-9506 at 270°C are shown in Fig. 7. At low frequency, the PP-PF100 is more viscous than the PET-9506. The curves cross each other at around 4.5 rad/s. At higher frequency, the PET-9506 is more viscous. This indicates that the PP-PF100 is more shear sensitive compared to PET-9506 at the measured temperature. The storage moduli of PP-PF100 and PET-9506 are plotted against frequency as shown in Fig. 8. Over a wide frequency range (0.1–30 rad/s), the PP-PF100 exhibits higher elasticity than the PET-9506. The elasticity ratio is about one at 30 rad/s. The curves of loss modulus (G'') vs. frequency are shown in Fig. 9.

3.2. Morphology development in immiscible blends

The deformation and breakup of a single Newtonian liquid drop in a Newtonian liquid matrix in a simple shear flow was first studied by Taylor [17,18]. An expression for determining the size of the largest drop that exists in a fluid undergoing a deformation at any shear rate can be written as

$$d = \frac{4\Gamma(\mu_r + 1)}{\dot{\gamma}\mu_m\left(\frac{19}{4}\mu_r + 4\right)} \quad (2)$$

where d is the diameter of drop, Γ is the interfacial tension, $\dot{\gamma}$ is the shear rate, μ_r is the viscosity ratio (viscosity of dispersed phase/viscosity of matrix), and μ_m is the matrix phase viscosity.

The systems of interest in this study are quite different from Taylor's since both the dispersed phase and matrix are viscoelastic, and the shear field in the extruder is much more complicated than the simple shear field. However, Taylor's studies provide a basis for analyzing the results obtained from the experiments.

Distributing and/or dispersing a minor or secondary component in a major component that serves as a matrix accomplish polymer blending or mixing in extruders. The

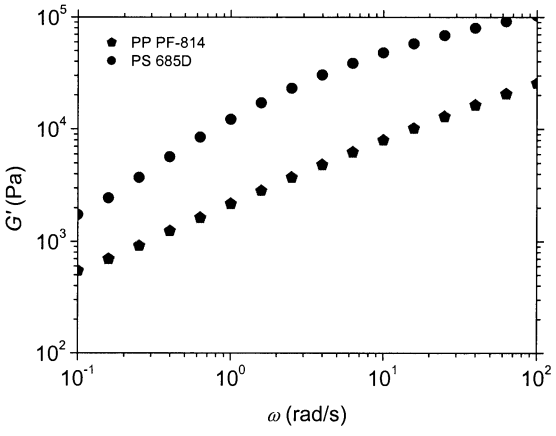

Fig. 2. Plots of storage modulus (G') vs. frequency (ω) of PP-PF814 and PS-685D at 200°C.

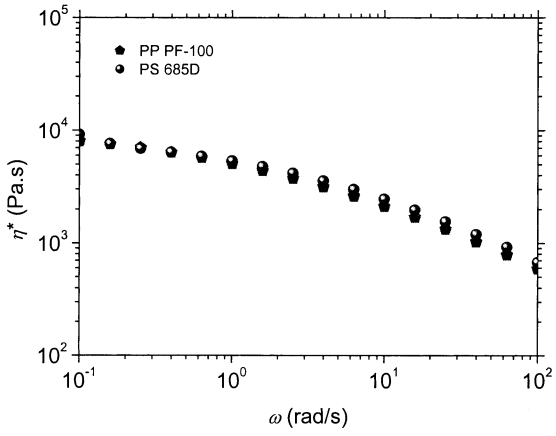

Fig. 4. Plots of complex viscosity (η^*) vs. frequency (ω) of PP-PF100 and PS-685D at 230°C.

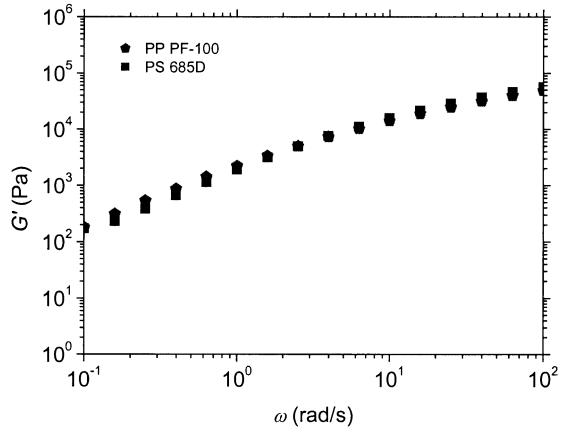

Fig. 5. Plots of storage modulus (G') vs. frequency (ω) of PP-PF100 and PS-685D at 230°C.

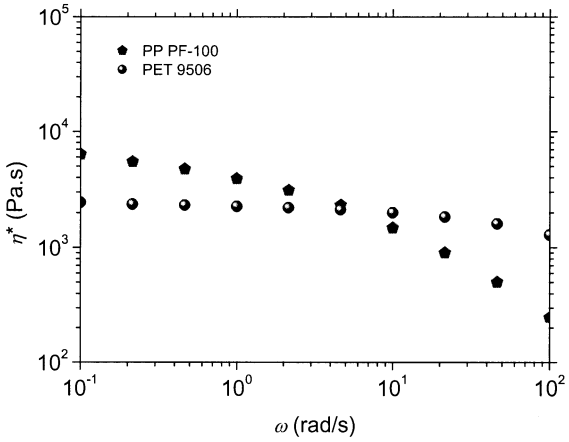

Fig. 7. Plots of complex viscosity (η^*) vs. frequency (ω) of PP-PF100 and PET-9506 at 270°C.

morphology development of immiscible blends is determined by competing distributive and dispersive mixing and coalescence mechanisms [16,19–21]. A parameter commonly used to determine whether a droplet will disperse is the capillary number defined by

$$\mathrm{Ca} \equiv \frac{\dot{\gamma}\mu_{\mathrm{m}}d}{2\Gamma} \tag{3}$$

where $\dot{\gamma}$ is the shear rate, μ_{m} is the matrix phase viscosity, d is the characteristic diameter of the droplet and Γ the interfacial tension that acts on the drop. The capillary number, Ca, is the ratio of flow stresses to droplet surface stresses. Breakup of the dispersed droplets is controlled by the viscosity ratio of the components and by the capillary number. Droplet break-up occurs when a critical capillary number, $\mathrm{Ca}_{\mathrm{crit}}$, is reached.

Grace [22] showed that for the breakup of Newtonian droplets in both simple shear and extensional flows, $\mathrm{Ca}_{\mathrm{crit}}$ depends on the type of flow and the viscosity ratio, μ_{r} (viscosity of dispersed phase/viscosity of matrix). For a viscosity ratio of one, the critical capillary number is in the range of 0.1–1 for both simple shear and elongational flows. As the viscosity ratio becomes larger than 4, simple shear flows cannot overcome the interfacial tension between the components and droplets cannot be broken up. Nevertheless, extensional flows do not exhibit any limit for drop breakup even at large values of viscosity ratio. Since elongational flow generates significantly higher stresses, it is more efficient in breaking up droplets. In addition, elongational flow is much more effective at distributive mixing. In order to achieve fine dispersed phase domains distributed in the matrix, both distributive and dispersive mixing are generally required. Dispersive mixing may be accomplished by exposing the material to extensional flow. A mixing device that provides aggressive, frequent, and time-varying shear and extensional flows such as an intermeshing twin-screw extruder is thus preferable vs. a single screw extruder for compounding immiscible polymers in order to attain a uniform mixture with fine level of dispersion.

The effect of viscosity ratio on the formation of the

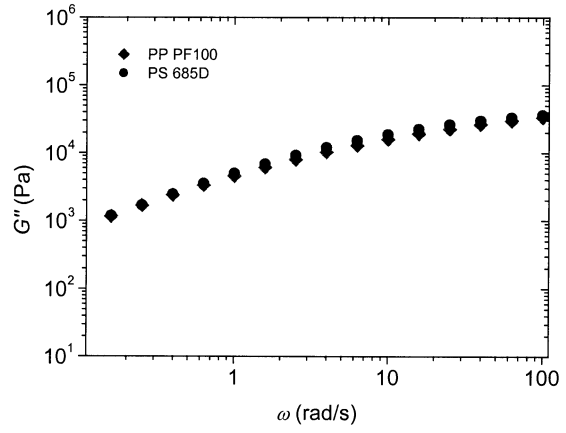

Fig. 6. Plots of loss modulus (G'') vs. frequency (ω) of PP-PF100 and PS-685D at 230°C.

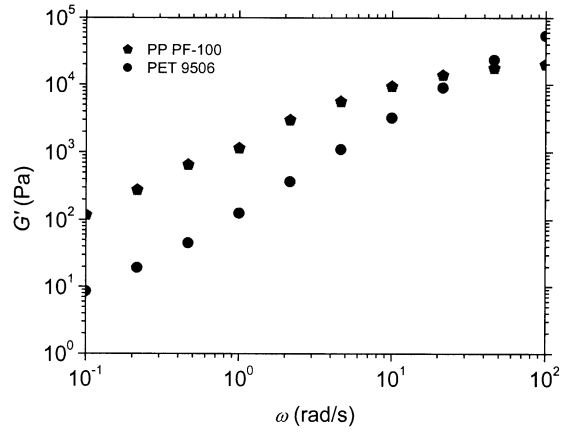

Fig. 8. Plots of storage modulus (G') vs. frequency (ω) of PP-PF100 and PET-9506 at 270°C.

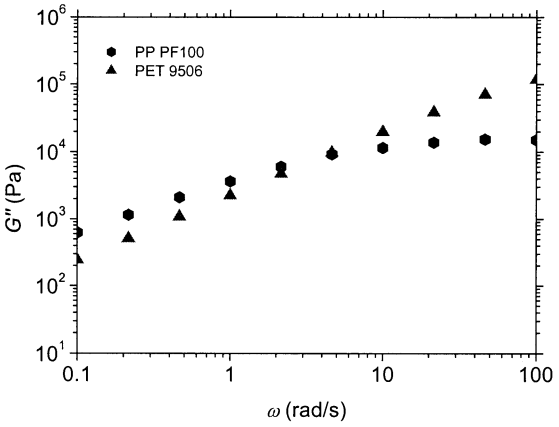

Fig. 9. Plots of loss modulus (G'') vs. frequency (ω) of PP-PF100 and PET-9506 at 270°C.

dispersed phase in immiscible blends during melt extrusion with a co-rotating twin-screw extruder has been extensively investigated by Wu [16]. Wu proposed to extend the Taylor's criterion to the case of a viscoelastic drop in a viscoelastic matrix. A correlation between dispersed-drop size and viscosity ratio, mostly valid for concentrations around 15 wt% of minor phase, was developed to estimate the average particle diameter obtainable for a given polymer pair. Wu's correlation is given in Eq. (4).

$$d = \frac{4\Gamma\mu_r^{\pm 0.84}}{\dot{\gamma}\mu_m} \tag{4}$$

where the plus (+) sign in the exponent applied for $\mu_r > 1$ and the minus (−) sign applied for $\mu_r < 1$. $\dot{\gamma}$ is an effective shear rate during extrusion taken as equal to the rpm. The shear rate in the fluid mechanical formulations, extending also to the above equations for polymer blends, under nearly all flow conditions assumes that the melt velocity equals that of the solid surface (equipment walls) [23]. This 'no-slip' assumption implies that the liquid adheres, and, thus, has no velocity relative to the wall. This assumption is in excellent agreement with both simulated and experimental results for the vast majority of polymers and processing flows at conditions below the region of the 'melt fracture' instability regime.

In addition to viscosity and elasticity ratios of the blend components, mixing mechanisms, shear rate, composition and interfacial tension play an important role in morphology development as suggested by Eq. (4). The size and shape of the dispersed phase are controlled appreciably by the interfacial tension. The morphology of blends with high interfacial tension is usually coarser than the morphology of blends with lower interfacial tension. In this work, interfacial tension values between the two blend components were estimated from surface tension values and polarities obtained from literature data [24–26]. Parameters used for the calculations are as follows:

Parameter	PP	PS	PET
Surface tension, Γ (mN/m)	21.9 (180°C)	29.2 (180°C)	28.3 (270°C)
Polarity, x^p	0	0.168	0.221
$-(d\Gamma/dT)$ (mN/m/°C)	0.040	0.072	0.065

The harmonic-mean equation is given by

$$\Gamma_{12} = \Gamma_1 + \Gamma_2 - 2\phi(\Gamma_1\Gamma_2)^{1/2} \tag{5}$$

where ϕ is the interaction parameter defined as:

$$\phi = \frac{2x_1^d x_2^d}{g_1 x_1^d + g_2 x_2^d} + \frac{2x_1^p x_2^p}{g_1 x_1^p + g_2 x_2^p} \tag{6}$$

$$g_i = \left(\frac{\Gamma_i}{\Gamma_j}\right)^{1/2} = \frac{1}{g_j} \tag{7}$$

$$x_i^p = \frac{\Gamma_i^p}{\Gamma_i} \tag{8}$$

where x_i^p is defined as the polarity, and $x_i^d + x_i^p = 1$; the superscripts d and p refer to dispersion (non-polar) and polar components, respectively.

$$x_j^p = \frac{\Gamma_j^p}{\Gamma_j} \tag{9}$$

The interfacial tensions of PP/PS at 200 and 230°C and PP/PET at 270°C as calculated from the harmonic-mean equation are fairly high and typical of immiscible polymer systems:

$\Gamma_{PP/PS}$ at 200°C (mN/m)	$\Gamma_{PP/PS}$ at 230°C (mN/m)	$\Gamma_{PP/PET}$ at 270°C (mN/m)
4.8	4.3	6.6

As shown, the magnitude of interfacial tension is determined primarily by the disparity in the polarities of the two phases. The greater the polarity difference, the greater will be the interfacial tension. The adhesive strength between two phases is also determined by the extent of interfacial contact and the extent of irreversible deformations occurring in the high stress concentration zone.

From the above discussion it is clear that in the absence of any additional compatibilizing species that reduce interfacial tension and result in finer dispersed domain size [27], the binary PP/PS and PP/PET blends of this work will have relatively coarse morphologies. Morphologies will be, to a large extent, dependent on component melt rheology at process conditions and blend composition. It is expected that by controlling the blend morphology, the microstructure of the microporous membranes prepared by stretching could also be tailored to a specific need.

3.3. Morphology of immiscible blends

3.3.1. Polypropylene/polyester blends

For the combination of PP-PF100 and PET-9506 melt blended at 270°C in the twin-screw extruder, the viscosity ratio ($\eta^*_{PET9506}/\eta^*_{PF100}$) at the operating temperature is about 1.4 at the effective shear rate. Scanning electron micrographs of fracture surfaces of 85% PP-PF100/ 15% PET-9506 shown in Fig. 10 are typical of immiscible systems. Because of the polarity differences PET does not spread on PP resulting in spherical PET particles. The adhesion between two components appears to be poor, as expected. Different sizes of PET particles co-exist in the blend. The dispersed phase domain sizes are ranging from 0.6 to 9.7 μm with an average size (d_n) of about 2.7 μm. A rather broad dispersed phase size distribution curve for this blend is shown in Fig. 11 where the number of dispersed phase domains is plotted as a function of the domain dimensions, d_p.

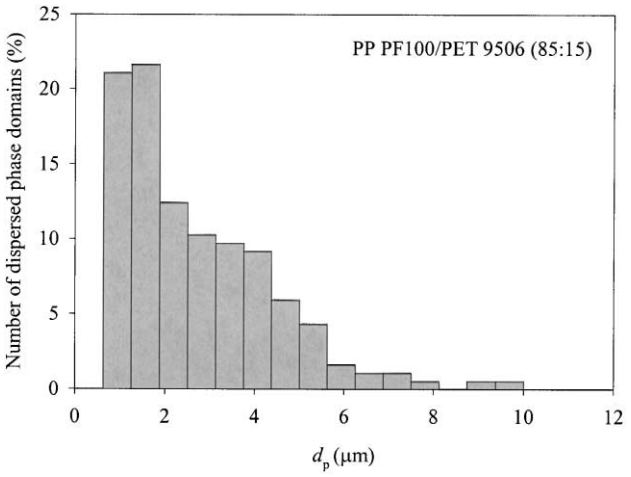

Fig. 11. Minor phase size distribution of PP-PF100/PET-9506 blend (85/15 wt%).

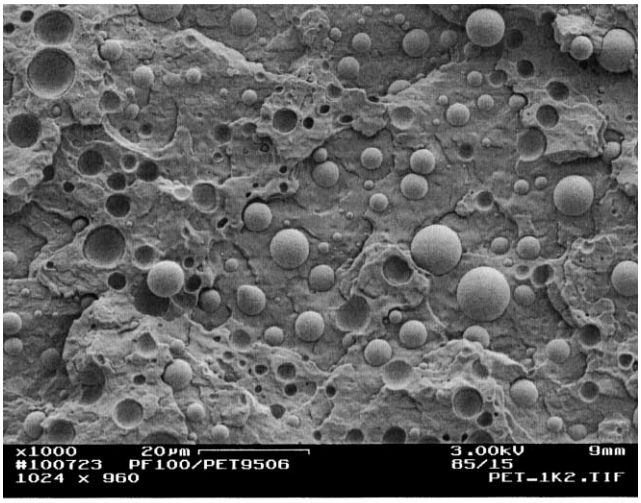

(a)

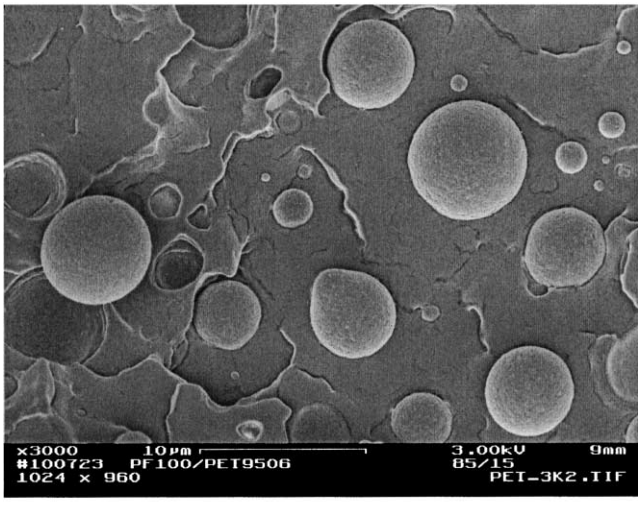

(b)

Fig. 10. Scanning electron micrographs of fracture surfaces of 15% PET-9506/85% PP-PF100 blend: (a) ×1 K; (b) ×3 K.

3.3.2. Polypropylene/polystyrene blends

Two polypropylene/polystyrene blends were selected as model systems to study the effects of minor phase concentration and viscosity ratio of the blend components on blend morphology. Specifically, blends of PP-PF100 and PS-685D were prepared with 1–10 wt% of polystyrene content to study the effects of the minor phase concentration on the blend morphology. PP-PF814/PS-685D was prepared at 90/10 wt% compositions to compare with the 90/10 wt% PP-PF100/PS-685D blend in order to elucidate the effects of viscosity ratio on blend morphology.

3.3.2.1. Effect of dispersed phase concentration on morphology. The size of the dispersed phase and the interparticle distance are crucial parameters in determining the mechanical behavior of blends and are controlled by dispersed phase concentration and drop breakup and coalescence phenomena during melt blending. For PP-PF100/PS-685D blends prepared at 99/1, 95/5, 90/10 weight ratios, compounding was carried out in the twin-screw extruder under fixed processing conditions in order to evaluate the influence of composition on dispersed phase domain size and estimate the extent of coalescence.

For the 99/1 wt% system a limiting domain size may be obtained since the coalescence of the minor phase is unlikely to occur. The effective shear rate of the extruder was of the order of 60 s^{-1}. The viscosity ratio of the two components ($\eta^*_{PS\text{-}685D}/\eta^*_{PF100}$) at the operating temperature is about 1.2 at the effective shear rate. Scanning electron micrograph of a fracture surface of the blend is shown in Fig. 12(a). The dispersed phase domain sizes are ranging from 0.2 to 0.8 μm with an average size of about 0.37 μm.

A scanning electron micrograph of a fracture surface of the 95/5 wt% system is shown in Fig. 12(b). The dispersed

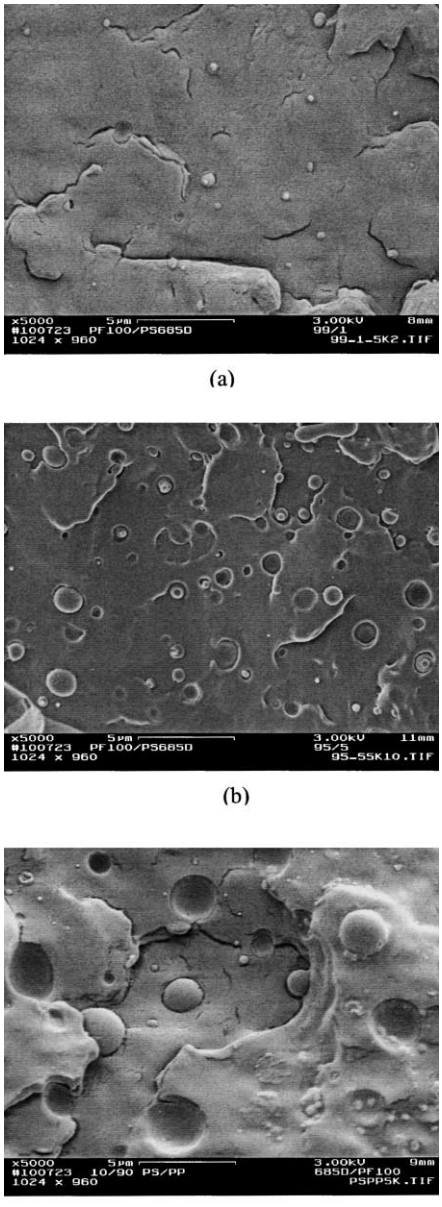

Fig. 12. Effect of dispersed phase concentration on blend morphology of PP-PF100/PS-685D blends: (a) 99/1, (b) 95/5, (c) 90/10.

phase domain sizes are ranging from 0.2 to 1.6 μm with an average size of about 0.54 μm. The average polystyrene particle size of the 95/5 PP/PS blend increases by 46 percent comparing to that of the 99/1 blend presumably due to increasing coalescence of the minor polystyrene phase.

A scanning electron micrograph of the fracture surface of the 90/10 wt% system is shown in Fig. 12(c). The dispersed phase domain sizes are ranging from 0.2 to 3.4 μm with an average size of about 0.95 μm. Because of the high surface tension of the dispersed polystyrene phase, the domains are nearly perfect spheres. The polystyrene particles appear to be well distributed in the polypropylene matrix at this composition. The adhesion between the two components is again poor because of the polarity difference between the two phases. The detachment of the particles from the polypropylene matrix is clearly visible.

The dispersed phase domain size distribution of the blends at different polystyrene concentrations is shown in Fig. 13. At 10 wt% minor phase, the blend exhibits much broader polydispersity compared to the systems containing 1 and 5 wt% minor phase. Thus, at higher dispersed phase concentrations, the coalescence is more pronounced and therefore leads, not only to increased average dispersed phase size, but also to broader particle size distributions. It should be noted that the uncompatibilized blend morphologies are unstable in the sense that flow induced coalescence may occur which coarsens the fineness of the dispersed phase. This is more pronounced for more concentrated blends since the flow induced droplet collisions leading to coalescence are much more frequent. However, the morphology during quiescent cooling may only be slightly affected since the droplets do not move to coalesce. Finally, the blend morphology is considered to be totally stable at room/use temperature.

Fig. 14 shows graphically the dependence of dispersed phase size on composition for the above PP/PS blends. There is a continuing increase of dispersed phase dimensions with increasing composition: d_n increases from about 0.4 to 1.0 μm when the polystyrene concentration is increased from 1 to 10%. At 1% dispersed phase concentration, only breakup should occur and therefore there should be a limiting drop size. At higher dispersed phase concentrations, the particles formed in the breakup process will usually collide and coalescence of the droplets may occur. The experimental results are compared with the Taylor limit, which describes the drop breakup in a Newtonian fluid (Eq. (2)) and Wu's correlation (Eq. (4)), which was obtained empirically. Disagreement with Taylor's results could be attributed to the fact that the Taylor limit does not account for the non-Newtonian effects that are present in the studied blend systems. However, at 1% dispersed phase concentration, the number average size of the dispersed phase of 0.37 μm is in satisfactory agreement with the value estimated from Wu's correlation (0.41 μm). In fact, Wu's correlation is always greater than the experimental limit since the correlation was obtained from blends with 15% weight fraction of dispersed phase, taking into account the effect of coalescence.

In summary, the coalescence of the minor phase of the 90/10 blend as shown by the larger domain diameter and polydispersity is much more pronounced compared to the 95/5 and 99/1 blends. The morphology of the blends clearly coarsens as the content of polystyrene increases in the range of dispersed phase concentrations investigated (1–10 wt%). It should be noted that the PP-PF100/PS-685D blend system having an interfacial tension of 4.3 mN/m has much finer dispersed phase (0.2–3.4 μm) compared to the PP-PF100/PET-9506 system (0.6–9.7 μm), with an interfacial tension of 6.6 mN/m; this is in spite of the approximately similar

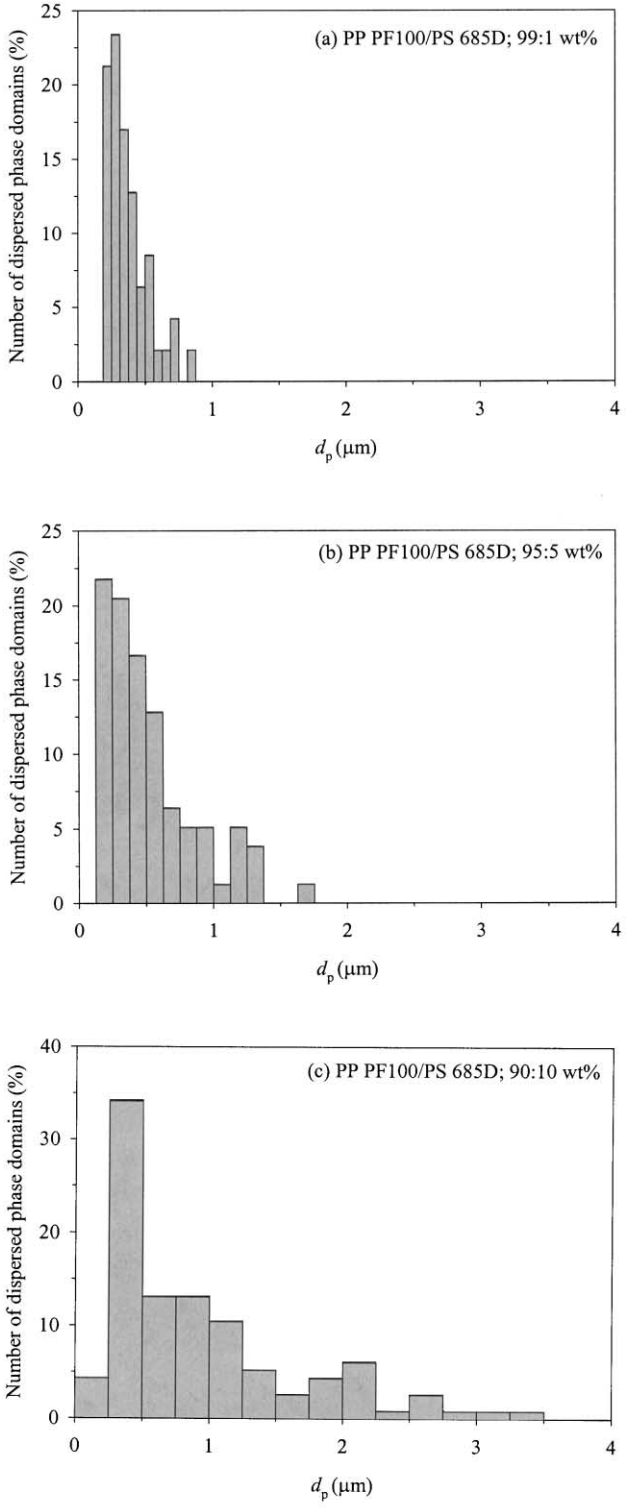

Fig. 13. Minor phase size distributions of PP-PF100/PS-685D blends with different minor phase compositions.

viscosity and elasticity ratios of the blend components at process conditions.

3.3.2.2. Effects of viscosity ratio on blend morphology. To elucidate the effects on viscosity and elasticity ratios on

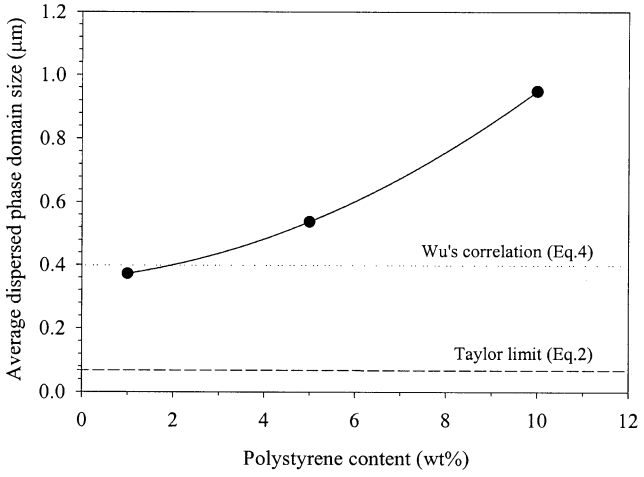

Fig. 14. Dependence of dispersed phase domain size on composition for PP-PF100/PS-685D blends.

systems with the same interfacial tension two different grades of polypropylene were used. For PP-PF814 and PS-685D melt blended in a twin-screw extruder at 200°C the viscosity ratio of the two components ($\eta^*_{\text{PS-685D}}/\eta^*_{\text{PF814}}$) at the operating temperature is about 5.1 at the effective shear rate (Table 2). Scanning electron micrographs of the fracture surface of the 90/10 blends are shown in Fig. 15. The polystyrene dispersed phase domain sizes range from 0.2 to 3.6 μm with an average size of about 1.5 μm. The shape of the polystyrene particles is irregular (angular polygonal) instead of spherical. This is indicative of the high elasticity of polystyrene that makes the particles difficult to deform. Inclusion morphology is evident in this blend system. Because of polarity difference between the two phases, polystyrene does not appear to adhere well to the polypropylene matrix.

For PP-PF100 and PS-685D melt blended at 230°C in a twin-screw extruder the viscosity ratio of the two components ($\eta^*_{\text{PS-685D}}/\eta^*_{\text{PF814}}$) at the operating temperature is about 1.2 at the effective shear rate (Table 2). The morphology of the 90/10 blend (Fig. 12(c)) consists of dispersed domains of polystyrene in polypropylene with sizes ranging from 0.2 to 3.4 μm with an average size of about 0.95 μm. The average polystyrene particle size of the PP-PF100/PS-685D blend decreases by 57 percent compared to that of PP-PF814/PS-685D blend at the fixed 10 wt% minor phase concentration. In addition to the significant effect of viscosity ratio on

Table 2
Viscosity data of polypropylene and polystyrene materials

Material	η^* at the effective shear rate (60 s^{-1}) (Pa s)
Polypropylene PF814	1128 (at 200°C)
Polypropylene PF100	2113 (at 230°C)
Polystyrene 685D	5758 (at 200°C)
	2448 (at 230°C)

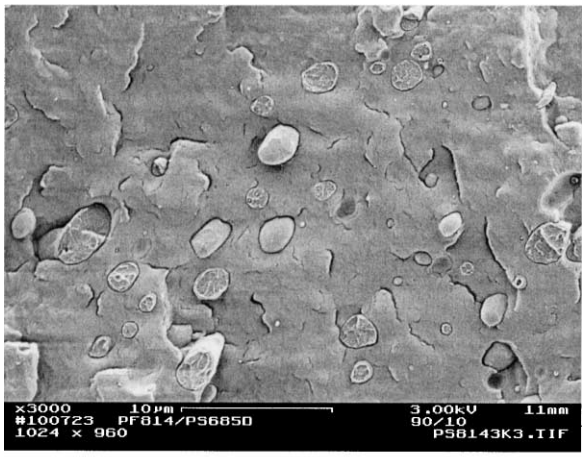

(a)

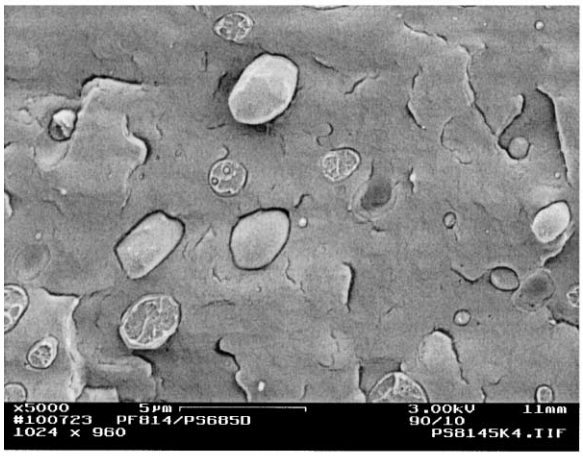

(b)

Fig. 15. Scanning electron micrographs of fracture surfaces of PP-PF814/PS-685D (90/10 wt%) blend: (a) ×3 K; (b) ×5 K.

the size of minor phase, the polydispersity in the size of the dispersed phase increases with increasing viscosity ratio (compare Figs. 16 and 13(c)). Note that in the 90/10 PP-PF814/PS-685D blends, there are a number of domains that are larger than 2 μm.

3.4. Microporous membranes based on immiscible binary blends

3.4.1. Membranes from polypropylene/polystyrene blends

The majority of the work on membrane formation was carried out with the equiviscous components PP-PF100/PS-685D blend (90/10 wt%) prepared by twin-screw compounding. The original thickness of the precursor non-porous film of 120 μm was reduced to a final thickness of the microporous film after the post-extrusion treatments of about 30 μm. After the blend films were stretched and heat-treated, they changed from opaque to milky-white indicating the formation of microcracks. The yielding area of the stretched film exhibited uniform stress whitening as its density decreases. A scanning electron micrograph of the

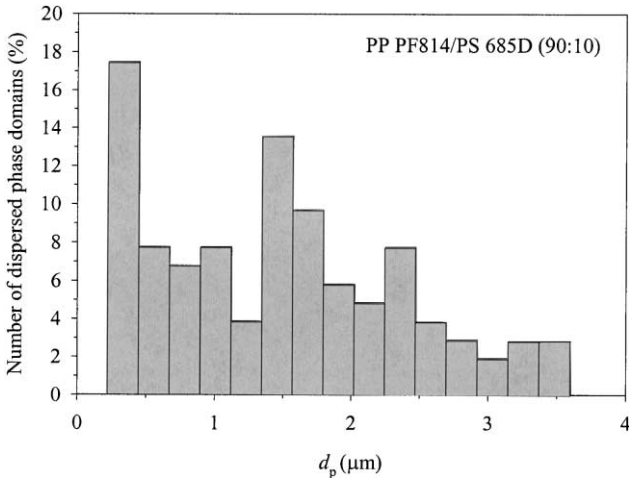

Fig. 16. Minor phase size distribution of PP-PF814/PS-685D blend (90/10 wt%).

surface of the film obtained after the post extrusion treatments shown in Fig. 17 reveals the formation of microcracks in the order of 6–8 nm in width. Fig. 18 shows a cross-section of the same membrane. Debonding at the interface between the major and the minor phase was observed at 3000× magnification (Fig. 18(a)) as a result of weak adhesion. At 50,000× magnification, Fig. 20(b), a network of microcracks uniformly distributed in the interior of the film was observed. The size of the microcracks found in the bulk is ranging from 4 to 8 nm.

When a two-phase polymer blend is subjected to mechanical deformation, the stress concentration inside the bulk of the material is amplified to a certain amount depending on location. A linear elastic solid finite element model was used to analyze the stress distribution inside the material around a dispersed phase domain acting as stress

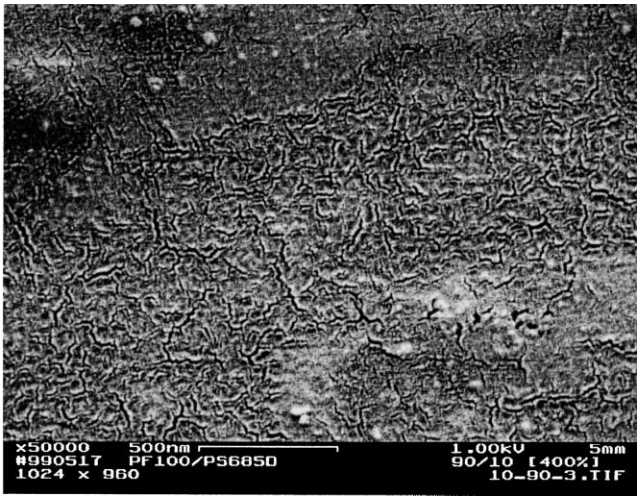

Fig. 17. Scanning electron micrograph of surface of microporous film based on 90/10 wt% PP-PF100/PS-685D blends prepared in the twin-screw extruder ×50 K.

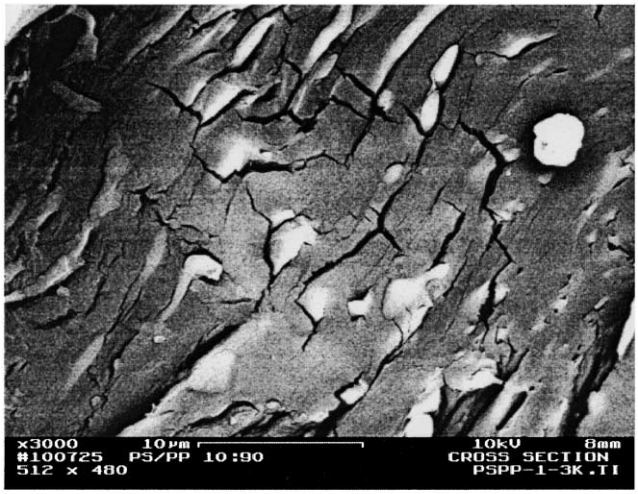

(a)

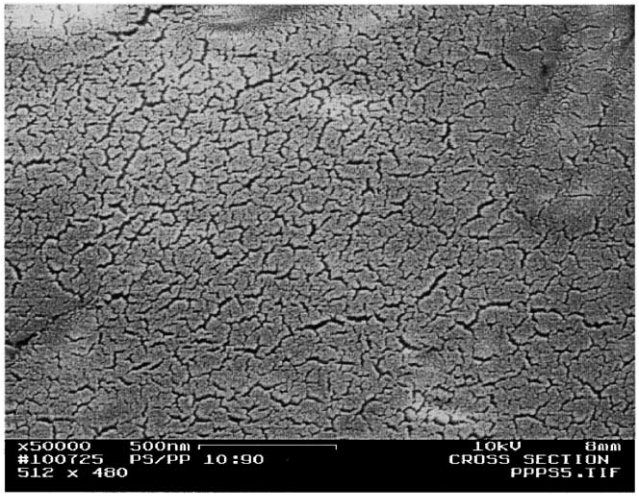

(b)

Fig. 18. Scanning electron micrograph showing a cross-section of microporous membrane based on 90/10 wt% PP-PF100/PS-685D blend prepared in the twin-screw extruder ×3 K (above); ×50 K(below).

concentrator in order to find a criterion for microcrack formation. The model of a 90/10 PP/PS binary blend containing multiple dispersed rigid PS domains in a PP matrix subjected to a uniaxial tensile load is illustrated in Fig. 19. The models were constructed to estimate the average stress field of randomly oriented inclusions embedded in the matrix. All dispersed phase domains were assumed to have similar size and shape. Since the inclusions are randomly distributed, the overall average properties of the blend are considered isotropic. Von Mises stress was used as a criterion for the microcrack formation with the tensile stress, σ_0 applied in the z-direction. The average stresses in both the matrix and inclusions generated by the deformation were calculated and the effects of the dispersed phase domains were quantitatively evaluated.

A quantitative result for the average stress was obtained with a commercial stress analysis software (ANSYS). As shown in Fig. 19, the interactions of the stress fields near each domain appear to lead to an increase of the shear stress in the bulk ranging from 1.2 to 1.5 times the applied stress. If the applied stress has a value higher than a critical limit to initiate the formation of microcracks, the model suggests that microcracks tend to initiate at the interphase boundary near the polar regions of the domains and grow outward into the continuous phase that has a high stress concentration. Details on the modeling procedure and the assumptions used may be found in Ref. [15].

In summary, the porosity in the precursor films is induced by creating the high stress regions in the films during the post-treatment by drawing the precursor film at a temperature below the glass transition temperature (T_g) of the minor phase. When the precursor film is deformed, the minor phase domains are debonded due to the weak adhesion between phases. Microscopy and finite element stress analysis suggest that microporous structures are formed by a crazing mechanism. Shear yielding also occurs along with the crazing. Microcracks are initiated at points of high stress concentration, which are at the interface between the two phases. Subsequent growth occurs by a process in

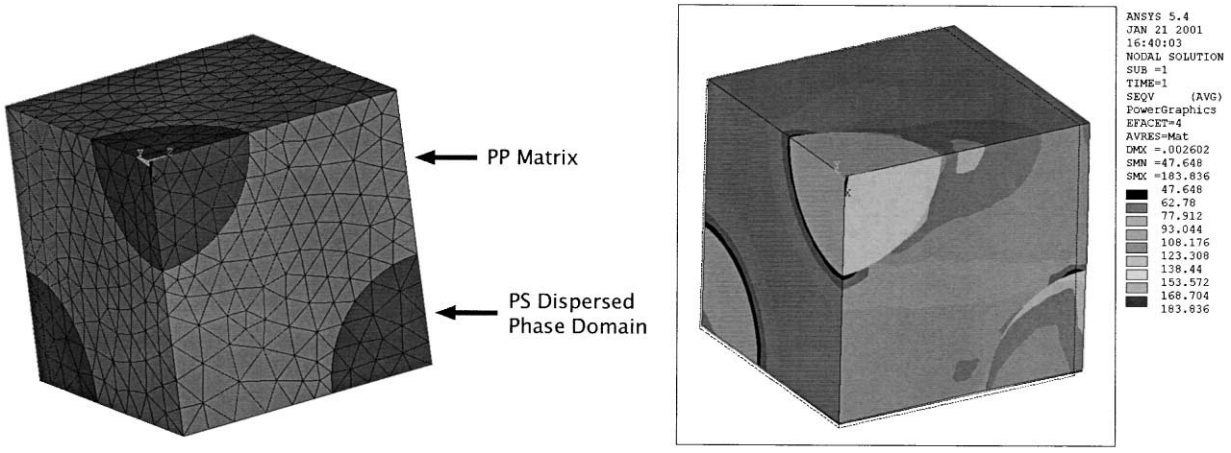

Fig. 19. Finite element modeling of 90/10 PP/PS blend to calculate stress distribution in the regions near the dispersed phase domains.

which crazes propagate into the major phase of blends. Rates of craze initiation and growth would then depend strongly upon the applied stress conditions and the drawing temperature.

In preliminary experiments, the effect of mixing on the membrane morphologies was studied on the two blend systems with components having different viscosity and elasticity ratios. 90/10 PF814/PS-685D ($\eta^*_{PS\text{-}685D}/\eta^*_{PP\text{-}PF814} = 5.1$) and 90/10 PF100/PS-685D ($\eta^*_{PS\text{-}685D}/\eta^*_{PP\text{-}PF100} = 1.2$) were extruded using a single screw extruder equipped with a sheet die in a one step operation followed by stretching. Although detailed morphological characterization data were not pursued, less intensive mixing in the single screw extruder was expected to produce blends with a much coarser morphology than the twin-screw extruder. The blend with the equiviscous components would still be expected to have smaller domain size and this would also affect the pore size and distribution of the stretched film.

Electron micrographs of the single extruder mixed blend surfaces (Fig. 20) show much larger pores than those of the twin-screw extruder surfaces (Fig. 17) with average size of 0.5 μm for the system with dissimilar viscosities and smaller size pores ranging from 0.1 to 0.2 μm for the system with the equiviscous components. Poor mixing in the single screw extruder produces a pore structure that is somewhat similar to the structure found in an homopolymer polypropylene membrane (Celgard™), [2–5] where slit like pores originate from the highly oriented 'row-nucleated' structures that form under high melt stress conditions [27,28]. The polystyrene dispersed phase domains increase the local stress in the film when it is subjected to tension making the formation of a row-nucleated structure more favorable. With the combination of the row-nucleated structure and local stress concentration, the pores are formed in the interlamellar region. However, the overall porosity in the blend film with poor mixing is relatively low due to the fact that the formation of pores does not occur uniformly throughout the film.

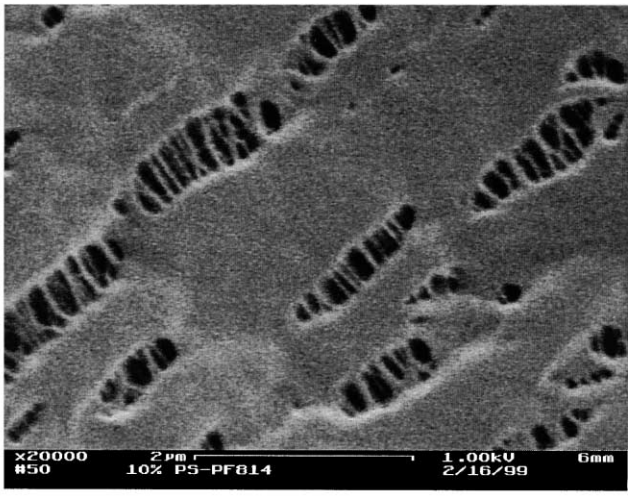

(a)

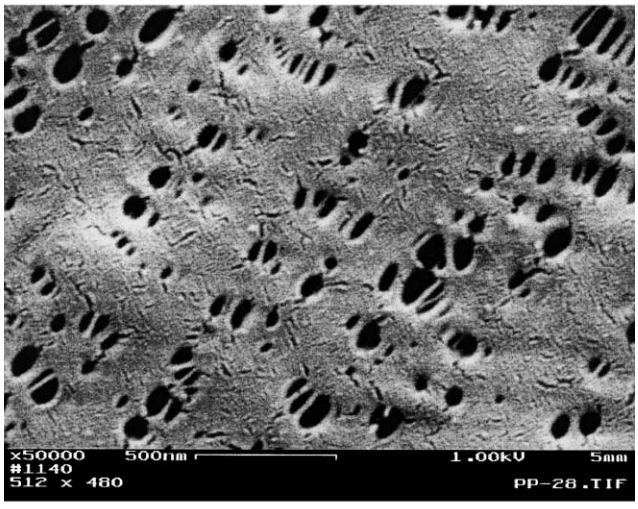

(b)

Fig. 20. Scanning electron micrographs of microporous PP/PS membranes prepared in single screw extruder: (a) (PF-814 /PS-685D; 10/90), × 20 K; (b) (PF-100/PS-685D 10/90) × 50 K.

3.4.2. Membranes produced from polypropylene/polyester blends

Microporous films were prepared from a non-porous precursor film of the PP-PF100/PET-9506 blend produced in the twin-screw extruder after uniaxially stretching by 400% at 25–30°C with respect to the original length. The original thickness of the precursor film of 120 μm was reduced to a final thickness of the microporous film of about 30 μm. As before the opaque precursor film was turned into a milky-white film after the post extrusion treatments. Scanning electron micrographs of the cross-section of the film obtained from the blend of PP-PF100/PET-9506 (85/15 wt%) are shown in Fig. 21. Debonding between the major and the minor phase was observed. At 100,000 × magnification (Fig. 21(b)), the structure of microcracks uniformly distributed in the interior of the film is clearly illustrated. The width of the fine microcracks is ranging from 2 to 4 nm which is somewhat lower than that found in the cross-section of the stretched films of the PP/PS blends prepared in the twin-screw extruder.

3.5. Membrane characterization by liquid permeation

Transport properties of membranes based on two blends obtained by twin-screw extrusion were characterized by permeability measurements. Permeability of a solvent through the microporous films was measured at different applied pressures ranging from 140 to 550 kPa (20–80 psi). It was found that the permeability increases linearly with increase in the applied pressure (Fig. 22). The permeability of the membranes based on two binary blends is ranging from 10^3 to 6.5×10^3 cm^3/(100 cm^2–day). It is

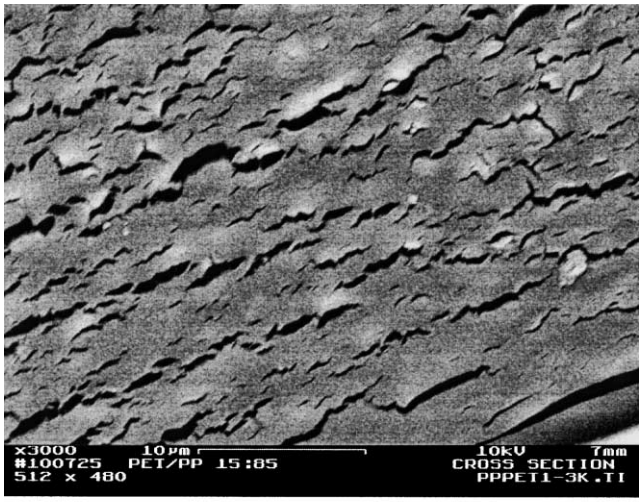

(a)

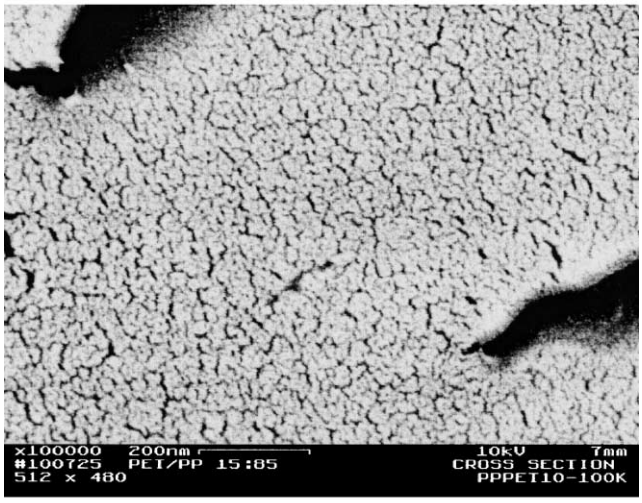

(b)

Fig. 21. Scanning electron micrographs showing cross-section of microporous membrane based on 85/15 wt% PP-PF100/PET-9506 blend prepared in twin-screw extruder: (a) ×30 K; (b) ×100 K.

shown that the permeability of the PP/PET blend membrane is higher than that of the PP/PS blends having a finer dispersed morphology by almost a factor of two. This is most probably due to the higher porosity of the film interior created by the plastic deformation during the post-extrusion treatments. Evidence of the latter was obtained in higher magnification electron micrographs of the PP/PET membrane (Fig. 21(b)). All the membranes produced via the melt process could withstand a significant pressure drop of 690 kPa applied for 72 h with no change in their properties.

The 90/10 PP/PS membranes were characterized for surface and cross-sectional pore characteristics. Mean surface pore diameter was 10.1 nm (4.4 nm minimum–15.7 nm maximum) with 11.1% surface porosity, values comparable to those of commercial phase inversion

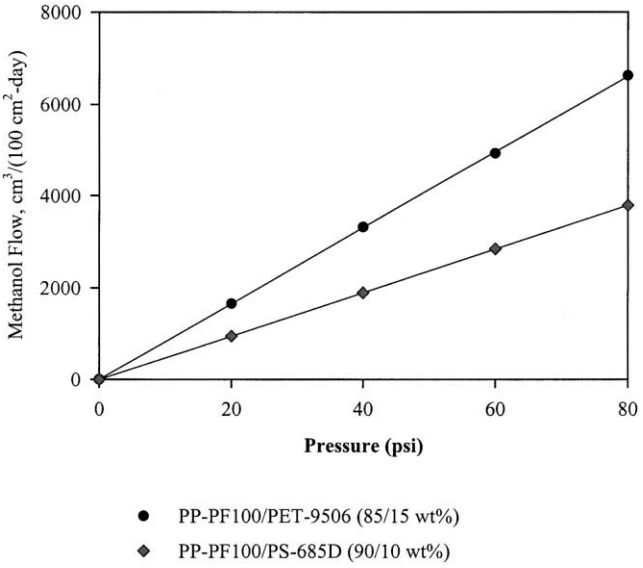

Fig. 22. Plots showing permeability of methanol through microporous membranes based on two-phase immiscible blends at different pressures at 20°C: 90/10 PP-PF100/PS-685D membrane vs. 85/15 PP-PF100/PET-9506 membrane.

membranes [29]. Cross-sectional mean pore diameter (12 nm) and porosity (8.4%) were comparable to the above experimental surface values. More details on the characteristics of the prepared membranes can be found in Ref. [15].

4. Conclusions

The present study described immiscible binary polypropylene blend compositions and processes to produce microporous membranes that could be used for a variety of separations in the ultrafiltration range, as suggested from permeability measurements. The novel membranes with pore size ranging from 2 to 25 nm were produced via melt processing and post-extrusion treatments in the solid state. Systems containing polystyrene and polyethylene terephthalate as the minor phase components were employed as starting membrane materials at concentrations not exceeding 15 wt%. The blends were first compounded in a co-rotating twin-screw extruder and subsequently extruded through a sheet die to obtain the non-porous precursor films. These were uniaxially drawn (100–500%) with respect to the original dimensions at a temperature below the glass transition temperature of the minor phase to induce a microporous structure and then post-treated at elevated temperatures to stabilize the porous structure, which consisted of uniform microcracks in the order of a few nanometers in width. Type and concentration of the dispersed phase, degree of dispersion and component melt rheology were shown to have significant effects on the morphology of the solid blends affecting also the microstructure

of the porous membrane. Finite element modeling of the stretching operation in the solid state yielded a successful interpretation of the blend response to uniaxial tension that resulted in microcrack formation. The fabrication process developed in the present study is versatile and capable of producing membranes with pore size and porosity ranges comparable to those of phase inversion membranes. Melt processing has several advantages over other membrane fabrication processes, especially for solvent-resistant membranes: membrane structure can be tailored by adjusting blend components and/or process parameters; high production rates resulting in lower production cost. Work is underway to evaluate a broader variety of polymer blends having different physical and chemical properties as starting materials.

Acknowledgements

The authors would like to acknowledge the financial support from the Center for Membrane Technologies at the New Jersey Institute of Technology through a grant from the New Jersey Commission on Science and Technology and the financial and technical assistance of the Polymer Processing Institute. In addition, the authors would like to thank Montell Polyolefins for supplying the polypropylene resin used in this work and Prof. M. Libera of Stevens Institute of Technology, Hoboken, NJ for his assistance with the SEM characterisation.

References

[1] Lloyd DR, Kinzer KE, Tseng HS. J Membrane Sci 1990;52:239.
[2] Druin ML, Loft JT, Plovan SG. US Patent 3,801,404, 1974.
[3] Bierenbaum HS, Isaacson RB, Druin ML, Plovan SG. Ind Engng Chem Prod Res Dev 1974;13:2.
[4] Bierenbaum HS, Daley LR, Zimmerman D, Hay IL. US Patent 3,843,761, 1974.
[5] Brazinsky I, Cooper WM, Gould AS. US Patent 4,138,459, 1979.
[6] Chu F, Yamaoka T, Kimura Y. Polymer 1995;36:2523.
[7] Chu F, Kimura Y. Polymer 1996;37:573.
[8] Zhu W, Zhang X, Zhao Ch, Wu W, Hou J, Xu M. Polym Adv Technol 1996;7(9):743.
[9] Xu M, et al. US Patent 5,134,174, 1992.
[10] Fried JR. Polymer science and technology. Englewood Cliffs, NJ: Prentice Hall PTR, 1995. Chapter 12.
[11] Mizutani Y. Microporous polypropylene films and fibers. In: Karger-Kocsis J, editor. Polypropylene: an A–Z reference. Dordrecht, The Netherlands: Kluwer Academic Publishers, 1999. p. 476–89.
[12] Chandavasu C, Xanthos M, Sirkar KK, Gogos CG. Proc 58th Soc Plast Engrs Ann Tech Conf 2000;46:2458.
[13] Chandavasu C, Xanthos M, Sirkar KK, Gogos CG. J Plast Film Sheet 2000;16:288.
[14] Xanthos M, Chandavasu C, Sirkar KK, Gogos CG. Melt processed microporous films from compatibilized immiscible blends with potential as membranes. Polym Engng Sci 2001; accepted for publication.
[15] Chandavasu C. PhD Dissertation. Newark (NJ): New Jersey Institute of Technology, 2001.
[16] Wu S. Polym Engng Sci 1987;27:335.
[17] Taylor GI. R Proc Soc Lond 1932;138A:41.
[18] Taylor GI. R Proc Soc Lond 1934;146A:501.
[19] Favis BD, Willis JM. J Polym Sci B: Polym Phys 1990;28:2259.
[20] Shi ZH, Utracki LA. Polym Engng Sci 1992;32:1834.
[21] Utracki LA, Shi ZH. Polym Engng Sci 1992;32:1824.
[22] Grace HP. Chem Engng Commun 1982;14:225.
[23] Tadmor Z, Gogos CG. Principles of polymer processing. New York: Wiley, 1979. p. 124–5.
[24] Wu S. Polymer interface and adhesion. New York: Marcel Dekker, 1982. p. 98–104.
[25] Kamal MR, Lai-Fook R, Demarquette NR. Polym Engng Sci 1994;34:1823.
[26] Xanthos M, Young M-W, Biesenberger JA. Polym Engng Sci 1990;30:355.
[27] Xanthos M. Reactive compatibilization of polypropylene. In: Karger-Kocsis J, editor. Polypropylene: an A–Z reference. Dordrecht, The Netherlands: Kluwer Academic Publishers, 1999. p. 694–700.
[28] Garber CAA, Clark ES. J Macromol Sci-Phys 1970;B4:499.
[29] Kim KJ, Fane AG, Fell CJD, Suzuki T, Dickson MR. J Membrane Sci 1990;54:89.